Experimental Study on Deformation Characteristics and Active Earth Pressure against the Flexible Retaining Wall with Limited Width Soil in Foundation Pit

Xinnian Zhu, Weidong Hu, Yongqing Zeng, *Member, IAENG*, Tao Hu, Siqing Jiang and Weiwei Wang

***Abstract*—The characteristics of the failure sliding surface and the distribution of active earth pressure of limited-width soil behind the flexible retaining wall are significantly affected by the deformation mode and displacement of the retaining wall, which is the design key to the retaining wall supporting adjacent to the existing underground structure. For the non-cohesive sand, the cantilever outward deflection mode and the drum parabolic deformation mode of the flexible retaining wall are simulated. The model tests are carried out to explore the deformation characteristics of limited-width soil and the distribution law of earth pressure. The test results show that in the cantilever outward deflection mode of a flexible cantilever retaining wall, the rupture surface forms a linear slip surface, which gradually penetrates from top to bottom. With the increased aspect ratio, the ultimate rupture angle gradually decreases and tends to be stable, which is close to the calculated value of Rankine's method. The critical aspect ratio is 0.4 for loose soil and 0.3 for medium-dense soil. When the aspect ratio is 0.2, the slip surfaces are broken-line slip surfaces. Under the drum parabolic mode, the soil slip surface is roughly a linear fracture surface, which develops from bottom to top and finally penetrates; the measured rupture angle of loose soil with limited width is greater than the ultimate rupture angle calculated by Rankine's method. In comparison, the measured rupture angle of medium-dense soil is smaller than the ultimate rupture angle calculated by Rankine's earth pressure theory. The critical aspect ratio is 0.4 for both loose and medium-dense soils. An apparent polyline surface appears in limited-width medium-dense soil. Under the cantilever outward deflection mode, the earth pressure gradually increases with the depth. As a result, the earth pressure rises more than Rankine's solution at the lower soil layer. Under the drum parabolic mode, the earth pressure along the retaining wall height is distributed in an "R" shape. Under the two modes, with the increase of aspect ratio, the value of earth pressure gradually increases and becomes a stable state after exceeding the critical aspect ratio. The analysis results can provide a reference for designing and constructing a flexible retaining structure such as row piles, sheet piles and diaphragm walls.**

***Index Terms*—flexible retaining wall; cantilever mode; drum parabolic mode; shear strain; active earth pressure**

Manuscript received January 14, 2022; revised October 8, 2022. This work was supported in part by the Natural Science Foundation of Hunan Province of China under Grants 2017JJ2110 and 2022JJ40160, the Key Scientific Program of Hunan Education Department of China under Grant 20A228, the Innovation Project of Hunan Undergraduate Students under Grants S202110543056, S202212658009 and S202110543058, and the Teaching Reform Research Project of Hunan Institute of Science and Technology under Grants 2021B21 and 2022A34.

Xinnian Zhu is a lecturer in College of Civil Engineering and Architecture, Hunan Institute of Science and Technology, Yueyang 414000, China, (e-mail: 11999496@hnist.edu.cn).

Weidong Hu is a professor in College of Civil Engineering and Architecture, Hunan Institute of Science and Technology, Yueyang 414000, China, (corresponding author e-mail: 11996498@hnist.edu.cn).

Yongqing Zeng is a lecturer in College of Civil Engineering and Architecture, Hunan Institute of Science and Technology, Yueyang 414000, China, (e-mail: 1013433575@qq.com).

Tao Hu is a postgraduate student in College of Civil Engineering and Architecture, Hunan Institute of Science and Technology, Yueyang 414000, China, (e-mail:822111140449@vip.hnist.edu.cn).

Siqing Jiang is a postgraduate student in College of Civil Engineering and Architecture, Hunan Institute of Science and Technology, Yueyang 414000, China, (e-mail:822111140452@vip.hnist.edu.cn).

Weiwei Wang is a lecturer in College of Civil Engineering and Architecture, Hunan Institute of Science and Technology, Yueyang 414000, China, (e-mail:12013032@hnist.edu.cn).

I. Introduction

MANY flexible pile walls have been applied in engineering, such as diaphragm walls, sheet pile walls, and cantilever piles. It is used for deep foundation pits near underground structures, urban subway stations, and municipal pipe networks [1-3]. The soil with limited width is formed between the support and existing structure. The sliding failure surface and earth pressure distribution of the soil with limited width differ from those of the infinite soil [4-7]. Frydman et al. [8] and Take et al. [9] conducted centrifugal model tests with sand. The distribution mode of active earth pressure acting on the rigid retaining wall and the deformation law of limited-width soil behind the wall are proposed. These provide a valuable reference for the follow-up theoretical research.

Khosravi et al. [10] used micro-pressure sensors and particle image velocimetry technology to conduct model experiments on the active earth pressure and shear deformation characteristics of sand in the translation mode of rigid retaining walls. Yang et al. [11] performed active earth pressure tests with three displacement modes of rigid retaining walls. It includes modes of translation (T mode), rotation around the bottom of the wall (RT mode), and rotation around the top of the wall (RB mode). The failure mode is observed by the colored sand layering method. The failure surface of the fill is continuous and always located in the Coulomb failure surface. Zhu et al. [12] conducted experimental research on sliding surface and earth pressure characteristics under typical displacement modes. It is pointed out that the solution of classical theory tends to be conservative by considering the width of soil, displacement

mode, and displacement magnitude. Hu et al. [13] verified the ultimate rupture surface and active earth pressure calculation model under the translational mode of the rigid retaining wall through the model test of limited-width soil under the grading condition. Fang et al. [14] carried out an experimental study on limited-width soil under various displacement modes (T mode, RT mode, and RB mode). The distribution of active earth pressure and the sliding failure surface is deeply studied. Wang et al. [15, 16] studied the typical displacement modes of rigid retaining walls, and the soil shear strain and displacement were obtained using the image correlation method. Ying et al. [17] conducted a model test on the passive earth pressure of limited-width soil in translation mode, which proposed that the passive earth pressure at different depths is more significant than Coulomb's solution. The narrower the soil width, the higher the passive earth pressure. The passive earth pressure in the lower part of the retaining wall increases more obviously. The above research shows that the deformation characteristics and ultimate failure surface of limited-width soil significantly differ from those with infinite width. The magnitude, distribution, and height of the resultant action point of the active earth pressure are different. The earth pressure presents a nonlinear distribution along the retaining wall, greatly affected by the displacement magnitude and mode. The active earth pressure within a limited width is less than the infinite.

Because of the small thickness to depth ratio of a flexible retaining wall, the deformation mode of a flexible retaining wall is significantly different from that of a rigid retaining wall [18-21]. As shown in Fig. 1, the cantilevered retaining wall rotates around the bottom and forms a forward-bending deflection deformation mode, resulting in a triangular horizontal displacement. In addition, during the excavation of the foundation pit, the restraint (internal support or anchor rod) at the top of the pile wall will cause the abdomen of the wall to protrude into the pit. Thus, a drum shaped parabola deformation mode is formed, and the horizontal displacement curve is a parabola. Due to the influence of deformation mode and displacement, the earth pressure distribution and slip surface for flexible retaining walls vary considerably.

Existing experimental studies on active earth pressure and sliding failure surface of finite-width soils mainly focus on rigid retaining walls. However, there is still a lack of systematic research on the characteristics of soil slip surfaces and the distribution of earth pressure behind the flexible retaining wall. Hu et al. [22] analyzed soil deformation, failure characteristics, and passive earth pressure distribution in the forward deflection deformation mode of flexible retaining walls by carrying out model tests. Zhu et al.[23] conducted an experimental study on the failure characteristics of soil behind a flexible retaining wall in the passive drum parabolic mode and acquired the distribution law of passive earth pressure. To some extent, the model test presents the failure characteristics of the finite soil behind the wall and the passive earth pressure distribution law. However, there are still few reports on the experimental studies on the active earth pressure and the characteristics of the slip surface of the finite-width soil behind the flexible retaining wall. There are crucial theoretical research and engineering application values in such experimental research.

Based on the above, this paper uses non-cohesive sand to carry out the finite-width soil model test of a flexible retaining wall under the cantilever flexural deformation mode and the drum parabolic mode. A high-speed camera was used to record the continuous deformation images of soil. The displacement, shear strain, and sliding failure surface with different aspect ratios were analyzed using the Digital Image Correlation (DIC) method [24-26]. The micro-earth pressure meter is used to measure the active earth pressure, which provides a reference for exploring the earth pressure distribution and theoretical calculation methods.

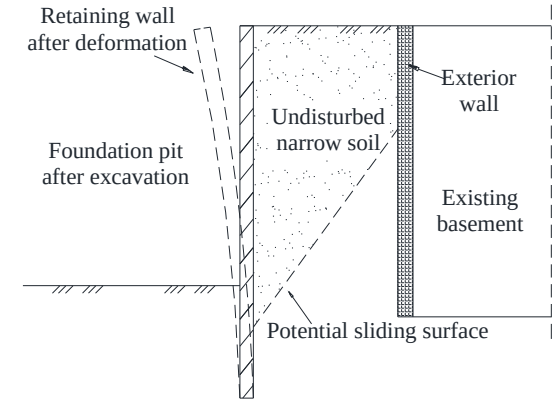

(a) Cantilever outward deflection mode

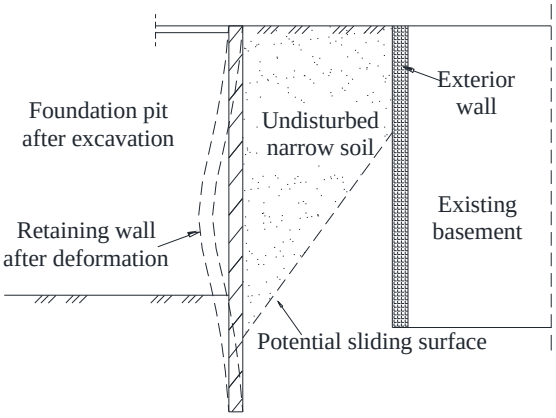

(b) Drum parabolic mode

Fig.1. Deformation mode of flexible retaining wall near existing basement

II. Model Test

A. Test Device

As shown in Fig. 2, the test box is made of steel. The size of length, breadth, and height are 1200mm, 425mm, and 700mm, respectively. The movable retaining wall on the left side of the earth box is made of a polypropylene plate, pasted with sandpaper to simulate a rough retaining wall. The fixed retaining wall on the right side of the earth box is made of steel plate with 12mm thickness, simulating existing fixed boundaries such as the outer wall of the existing underground structure. Usually, the surface of an underground concrete structure is relatively flat, so the steel plate surface remains in a semi-rough contact state with the soil without treatment. The front side of the model box is equipped with transparent tempered glass; the rear side is made of steel plate. The gap between the left and right wall panels is sealed with soft wool strips; lubricating oil is applied between the front and rear

wall panels and the soil. The width of soil can be adjusted by changing the position of the retaining wall in the steel box.

Fig. 2. Test model box

During the test, the limited-width soil behind a wall was used as the analysis area; a high-speed camera was used to take pictures automatically. Ensure the camera is perpendicular to the measurement surface and the light source is placed on both sides of the test box to reduce specular reflection. The shooting time interval was 0.5~1.0s, and the analysis was performed using digital image correlation analysis technology (DIC) and GOM Correlate software [24-26].

B. Displacement Mode

Two upper and lower three-phase motors are arranged outside the movable retaining wall. The motors are connected to the moveable retaining wall through the transmission shaft. The loading control box can automatically realize the movement of the moveable retaining wall by controlling the motor. According to the rotation speed of a motor, the rated translation speed for moving the top of the moveable retaining wall away from the soil is 0.2mm/s. In addition, a spring pressing rod and a spring pulling rod are arranged in the middle of the outer side of the movable retaining wall, which can apply horizontal pressure and tension to the middle of the movable retaining wall. Polypropylene plate has good resilience and can produce large elastic deformation. Horizontal loading can show inward arc deformation to simulate better the deflection mode of flexible retaining walls in foundation pit excavation.

As shown in Fig. 3, when simulating the outward deflection of the cantilever retaining wall, the lower motor does not run to simulate the bottom of the retaining wall is embedded and fixed. Furthermore, the upper motor drives the upper transmission shaft and rotates at a low speed, resulting in an inclined outward displacement of the movable wall. Meanwhile, a spring pressure rod is set in the middle of the wall. As a result, flexural deformation occurs while the movable wall inclines outward.

As shown in Fig. 4, in order to simulate that the top of the wall is constrained by internal support or anchor rod and the bottom of the wall is embedded in the soil, two motors do not operate. This way, the top and bottom of the wall will not have horizontal displacement. Instead, a spring pull rod is set in the middle of the movable wall so that the movable wall can move under the force of the rod to generate parabolic displacement.

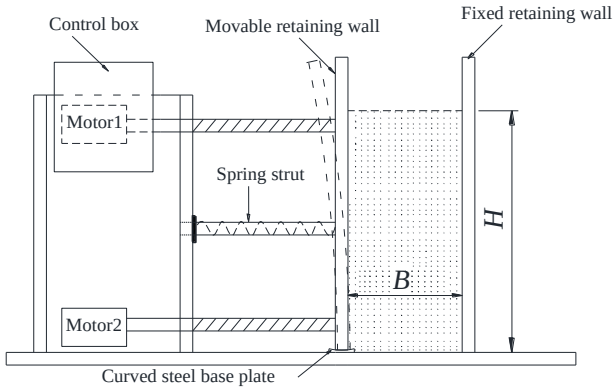

Fig. 3. Outward deflection motion mode of flexible cantilever retaining wall

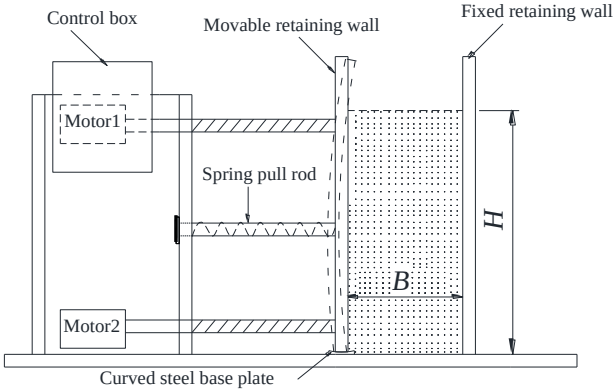

Fig. 4. Drum parabolic motion mode of flexible retaining wall

C. Earth Pressure Measurement

As shown in Fig. 5, five CYY9-type miniature earth pressure gauges are set on the movable retaining wall for measurement. The range, diameter, and thickness of earth pressure gauges are 5~10kPa, 22mm, and 13mm, respectively. Grooves are excavated along the vertical midline at the back of the movable wall for embedding gauges. The depth of the groove is consistent with the thickness of the earth pressure gauge to reduce the effect of the indicator on the flatness of the flexible wall.

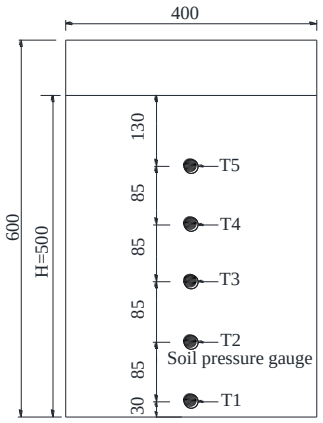

Fig. 5. Layout of earth pressure gauges（unit: mm）

During loading, the horizontal displacement value at the top of the movable wall is monitored in realtime by the dial indicator. In addition, the output voltages of the gauges are

collected in realtime by the acquisition instrument. The mean values of lateral earth pressures are tested and calculated under each level of displacement. The horizontal displacement values at different depths of the movable wall are tested after the wall stops moving.

D. Test Plan

(1) Soil sample preparation

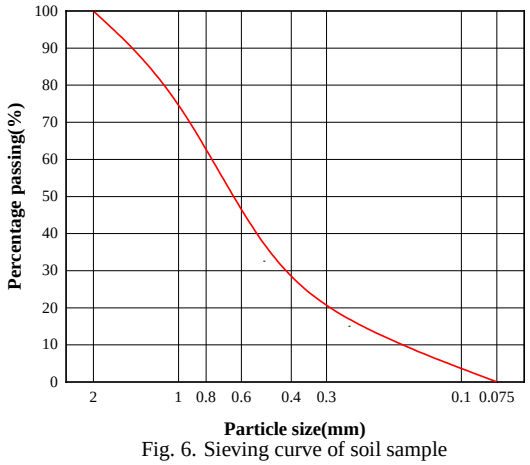

Fig. 6. Sieving curve of soil sample

The soil sample for the model test is non-cohesive sandy soil, which is prepared with the Dongting Lake sand. After cleaning, drying, and sieving, dry sand with a particle size of 0.075mm~2.0mm was selected as the test soil sample. The sieving curve of a soil sample is shown in Fig. 6. The mechanical parameters of the tested soil are as follows: cohesion=0, water content coefficient=0%, and other specific test parameters are shown in Table I.

Two sandy soils in loose and medium-dense states are prepared for testing. First, the test sand is filled in layers with a height of each layer of 50mm to realize the loose condition. To achieve the medium-dense state, after each layer of falling sand is filled with 50mm, the same standard is adopted for compaction layer by layer. After filling, it must stand for more than 3 hours to eliminate the difference in layered compaction.

(2) Test schedule

TABLE I
PROPERTIES OF THE TESTED SOIL

Test number	Density (g/cm^3)	Void ratio	Water content coefficient	Internal friction angle(°)
Loose	1.345	0.85	0	33.9
Medium -dense	1.541	0.66	0	41.9

This test mainly simulates two typical deformation modes of flexible retaining walls: one is the deformation displacement mode of forwarding deflection of cantilever flexible retaining wall; the other is the drum parabolic mode of the flexible retaining wall with supporting anchors. The research contents are the failure characteristics and the distribution law of earth pressure of sandy soil with limited width behind the flexible retaining wall. The total height of filling soil is 500mm. According to different aspect ratios (B/H) and compaction states, 24 tests were carried out. The experimental arrangement is shown in Table II.

III. SOIL DEFORMATION AND SLIDING FAILURE SURFACE

The soil sliding failure surface, deformation, and displacement of the test area behind the wall are obtained using image analysis technology and GOM Correlate software to analyze test results [24-26]. The analysis results include shear strain, total displacement, horizontal displacement in the X direction, and vertical displacement in the Y direction.

A. Cantilever outward Deflection Mode

(1) Sliding failure surface

Fig. 7 and Fig. 8 are the shear strain nephograms of loose and medium-dense soil under different aspect ratios, respectively. The initial position of the slip surface rises slightly with the increase of aspect ratio, in which the shear strain of the sand on the upper slip surface is more significant. The sliding fracture surface is straight and gradually penetrates from top to bottom. For loose soil, the starting height of the sliding surface rises from 0.2H to 0.3H. The starting point of the sliding surface of medium dense sand rises from 0.15H to 0.2H, lower than loose sand.

TABLE II
TEST SCHEDULE

Serial number	State	Cantilever outward deflection mode			Serial number	State	Drum parabolic mode		
		The height of soil /m	The width of soil /m	B/H			The height of soil /m	The width of the soil /m	B/H
1#	Loose	0.50	0.10	0.2	13#	Loose	0.50	0.10	0.2
2#	Loose		0.15	0.3	14#	Loose		0.15	0.3
3#	Loose		0.20	0.4	15#	Loose		0.20	0.4
4#	Loose		0.25	0.5	16#	Loose		0.25	0.5
5#	Loose		0.30	0.6	17#	Loose		0.30	0.6
6#	Loose		0.35	0.7	18#	Loose		0.35	0.7
7#	Medium dense		0.10	0.2	19#	Medium dense		0.10	0.2
8#	Medium dense		0.15	0.3	20#	Medium dense		0.15	0.3
9#	Medium dense		0.20	0.4	21#	Medium dense		0.20	0.4
10#	Medium dense		0.25	0.5	22#	Medium dense		0.25	0.5
11#	Medium dense		0.30	0.6	23#	Medium dense		0.30	0.6
12#	Medium dense		0.35	0.7	24#	Medium dense		0.35	0.7

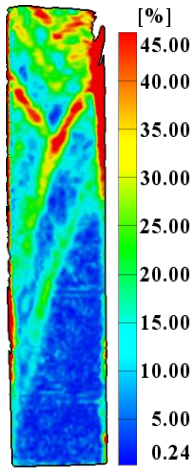

(a) B/H=0.2

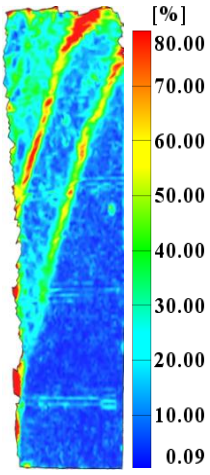

(b) B/H=0.3

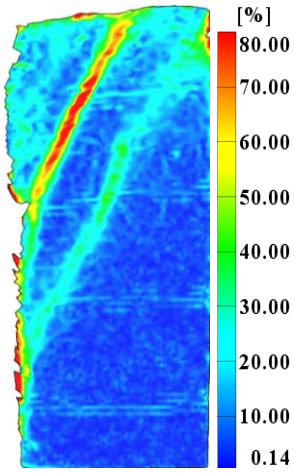

(c) B/H=0.4

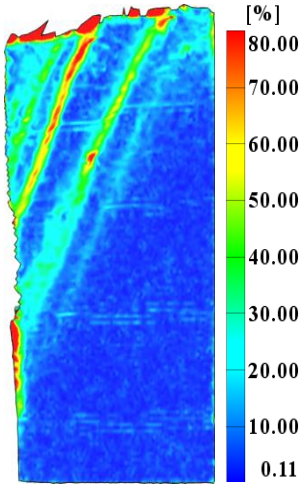

(d) B/H=0.5

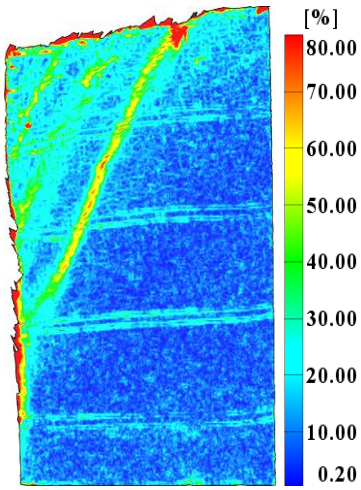

(e) B/H=0.6

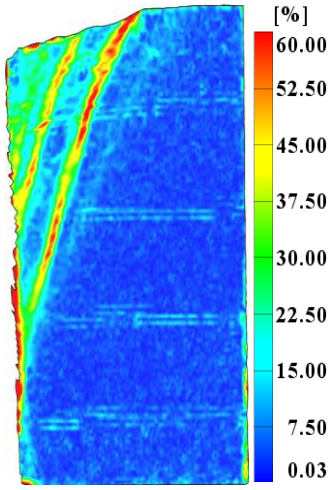

(f) B/H= 0.7

Fig. 7. Loose soil shear strain cloud map under Cantilever-mode

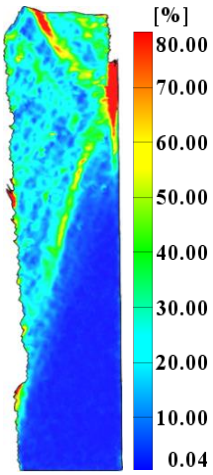

(a) B/H= 0.2

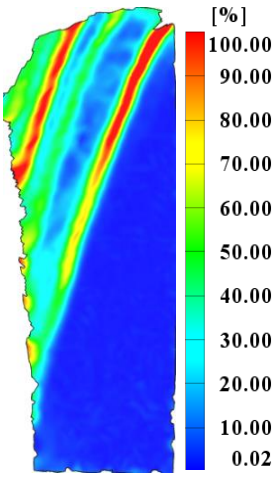

(b) B/H= 0.3

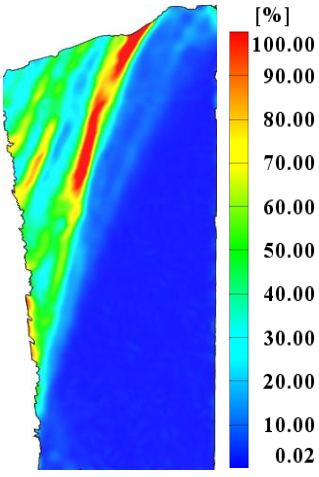

(c) B/H=0.4

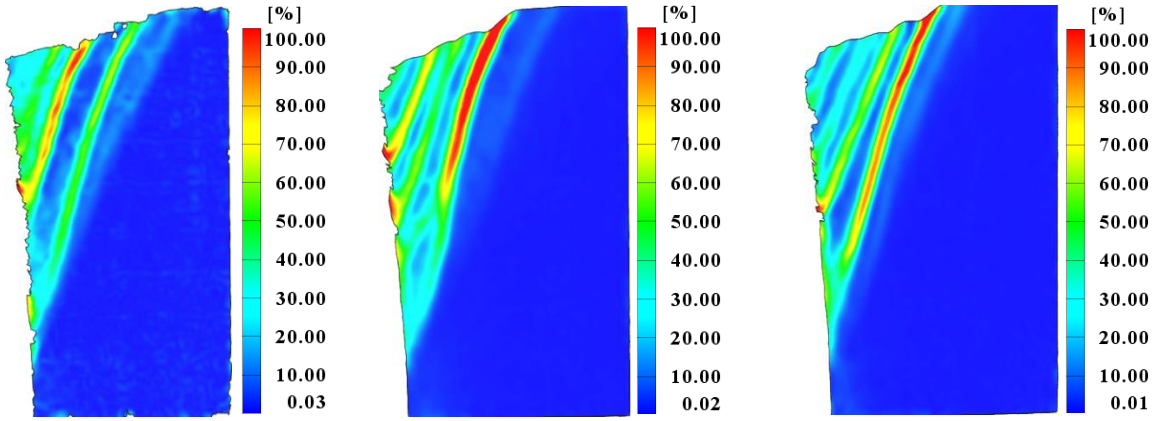

(d) B/H=0.5 e) B/H=0.6 f) B/H=0.7

Fig. 8. Medium dense soil shear strain cloud map under Cantilever-mode

For loose soil, when B/H is 0.5, 0.6, and 0.7, the slip surface slides out from the top surface of the soil; the soil deformation area is far from a fixed retaining wall, so it is judged as an infinite state soil. As shown in Fig. 7(c), when B/H is 0.4, the slip surface slips out from the junction point between the top surface of the soil body and the fixed retaining wall, which can be regarded as a critical state. Therefore, 0.4 is the critical aspect ratio. In Fig. 7(a) and Fig. 7(b), when B/H is less than 0.4, the slip surface terminates at the fixed retaining wall. The fixed retaining wall affects the slip surface and deformation, which can be considered soil with limited width. According to the same method, it can be judged that the critical aspect ratio of medium-dense soil is 0.3.

When the aspect ratio B/H=0.3, 0.4, 0.5, 0.6, and 0.7, two or more slip surfaces appeared in the loose and medium-dense soil. Figures 7(a) and 8(a) show that when B/H is 0.2, both loose and medium-dense soil has broken-line slip surfaces. The first main sliding surface is from 0.15H or 0.2H to 0.8H above the fixed retaining wall. The second main sliding surface is reflected from the endpoint of the first main slip surface in the upper part of a fixed retaining wall and extends upward to the top surface of the filling soil.

As shown in Table III, with the aspect ratio of loose and medium-dense soil increasing, the ultimate rupture angle gradually decreases and becomes stable. The model test results show that: according to Rankine's earth pressure theory, the ultimate rupture angle is 45 °+φ/2; the ultimate rupture angle calculated by the internal friction angle of loose soil and medium-dense soil is 61.95 °and 65.95 °, respectively. Fig. 9 is a characteristic comparison diagram of the shear slip surface of the soil under different aspect ratios in the cantilever deflection mode, in which Rankine's slip surface was added for comparison. The measured rupture angle of limited width soil is greater than the ultimate rupture angle calculated by Rankine's method ($\alpha = 45° + \varphi/2$); however, the measured rupture angle of soil entering infinite width is close to the ultimate rupture angle calculated by Rankine's method.

(2) Soil Deformation

As shown in Fig. 10, taking loose and medium-dense semi-infinite soils with B/H=0.7 as an example, the maximal total displacement, the maximal X-direction horizontal displacement, and the maximal Y-direction vertical displacement all appear near the top of the moveable retaining wall. In Fig. 10, the displacement magnitude gradually decreases downward, and the cloud image is similar. When B/H is 0.3, 0.4, 0.5, and 0.6, the slip surface and deformation characteristics are similar to those of semi-infinite soil. The total displacement, X displacement, and Y displacement have a similarity.

As shown in Fig. 11, when B/H is 0.2, the maximal total displacement and the maximal horizontal displacement in the X direction still appear near the top of the moveable retaining wall. Still, the maximal vertical displacement in the Y direction appears in the upper part of the soil layer. Therefore, the total displacement map, X displacement, and Y displacement cloud map are not similar.

TABLE III
FAILURE ANGLE OF SLIDING SURFACE (CANTILEVER-MODE)

Failure angle(°)	B/H=0.2	0.3	0.4	0.5	0.6	0.7	45°+φ/2 (°)
Loose	66.04	65.22	60.26	60.25	60.63	60.25	61.95
Medium dense	70.02	69.44	69.86	69.44	69.15	67.10	65.95

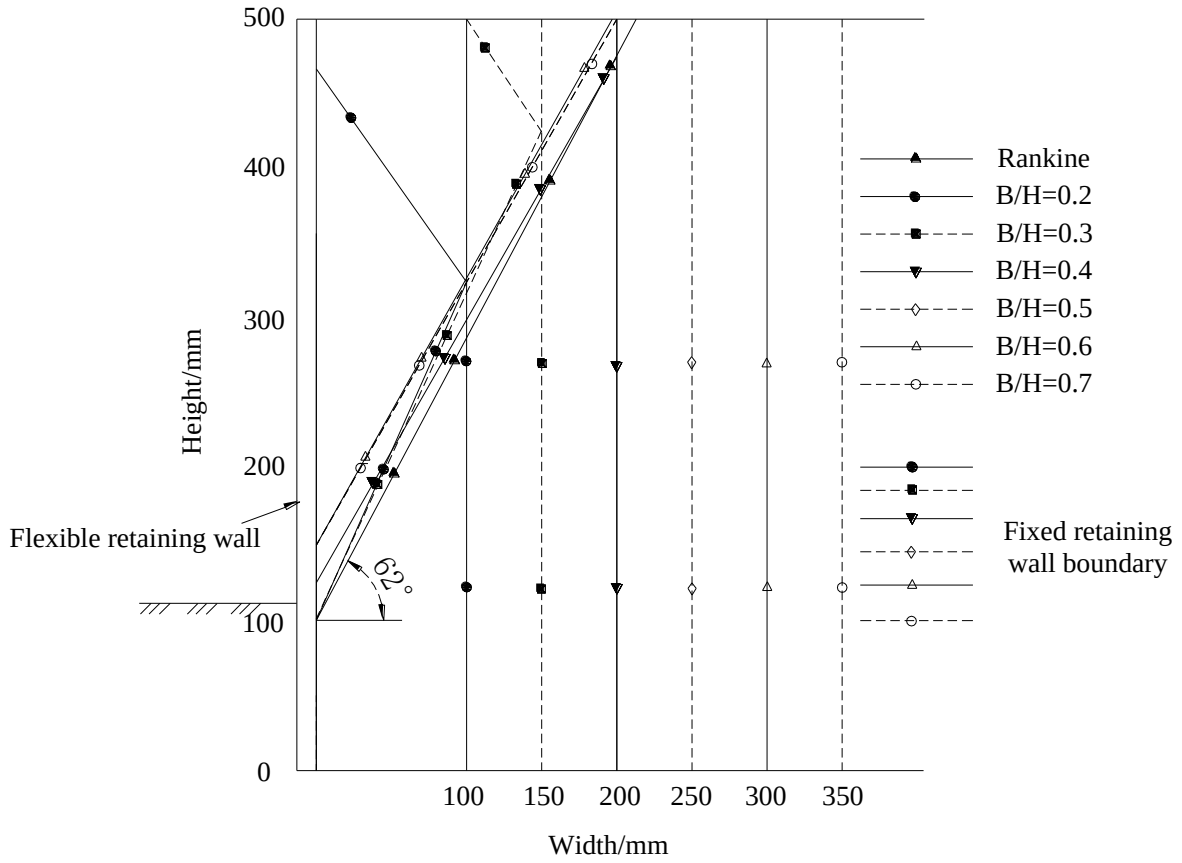

(a) Loose soil

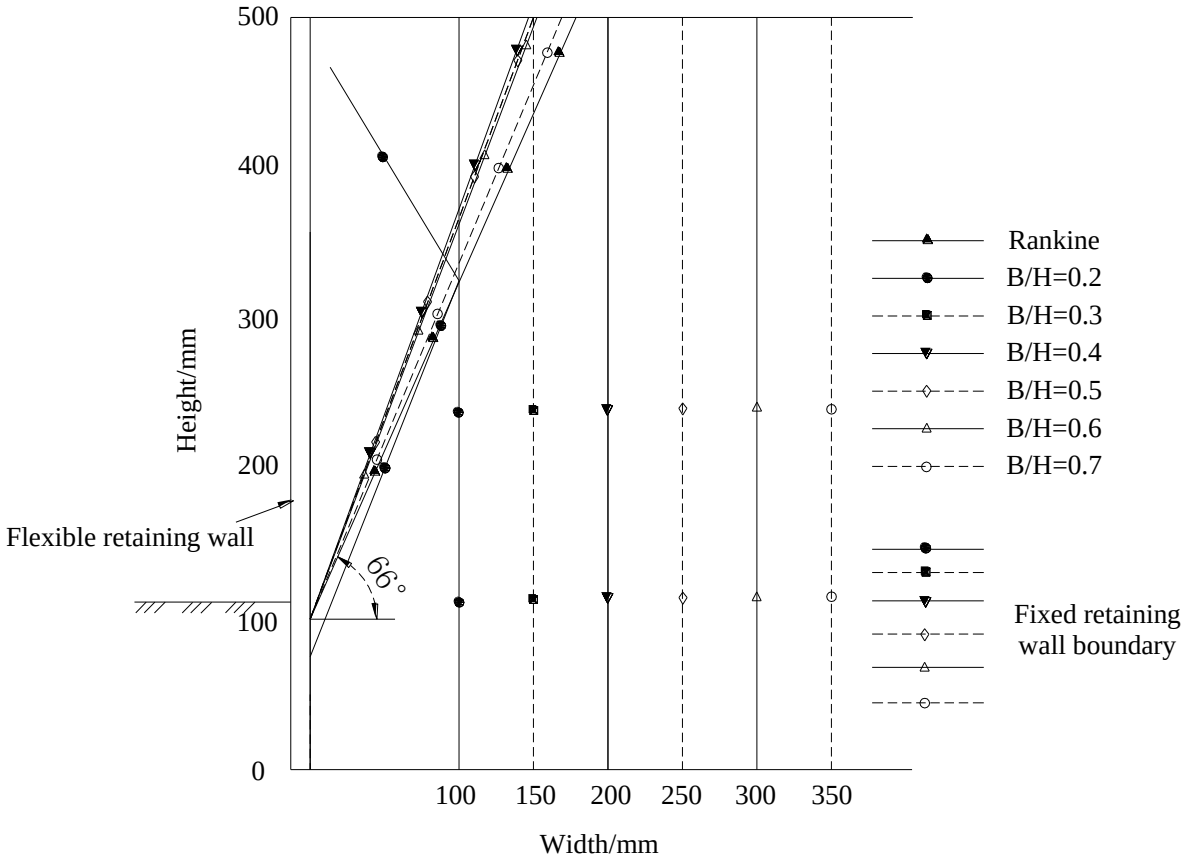

(b)Medium dense soil

Fig. 9. Characteristics of soil slip surface with different B/H under Cantilever-mode

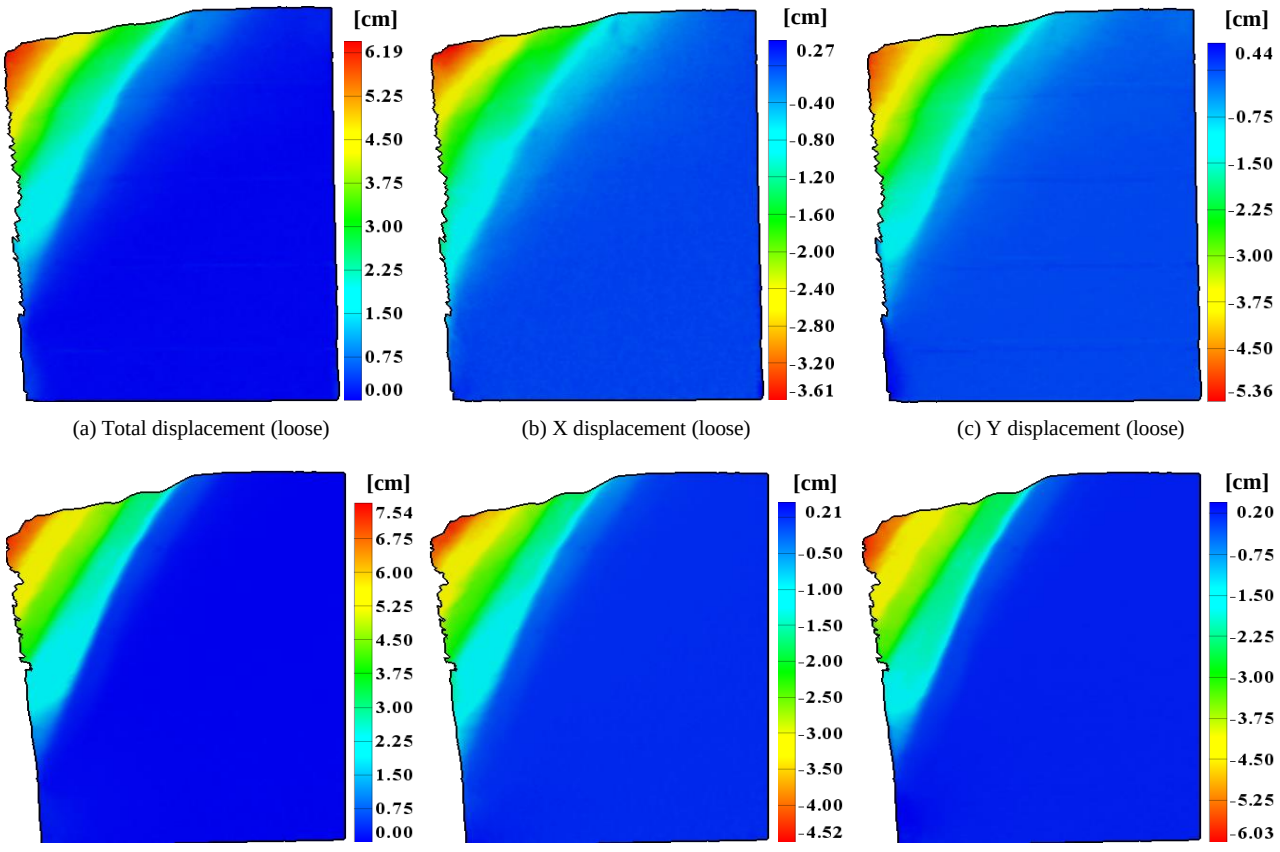

(a) Total displacement (loose) (b) X displacement (loose) (c) Y displacement (loose)

(d) Total displacement (Medium dense) (e) X displacement (Medium dense) (f) Y displacement (Medium dense)

Fig. 10. Soil deformation characteristics under Cantilever-mode (B/H=0.7)

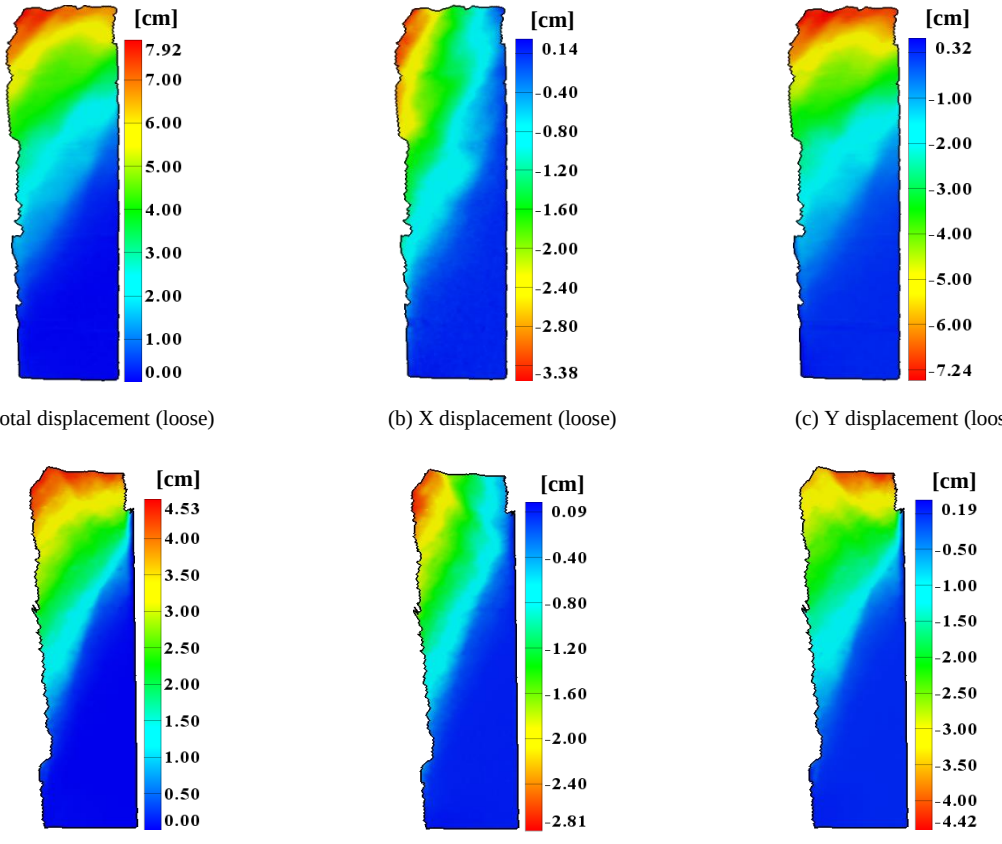

(a) Total displacement (loose) (b) X displacement (loose) (c) Y displacement (loose)

(d) Total displacement (Medium dense) (e) X displacement (Medium dense) (f) Y displacement (Medium dense)

Fig. 11. Soil deformation characteristics under Cantilever-mode (B/H=0.2)

B. Drum Parabolic Deformation

(1) Sliding failure surface

Fig. 12 and Fig. 13 are the shear strain diagrams of the drum parabolic mode of soil in the loose state and the medium-dense state, respectively. The slip surface is roughly a linear fracture surface, which develops from the bottom to the top and finally penetrates. As a result, the shear strain of soil at the lower slip surface is larger. However, the starting point of the surface is relatively stable. For loose and medium-dense soil, the starting point of the surface is located at the height of 0.2H~0.25H. As shown in Table IV, with the increase of the aspect ratio, the inclination of the slip surface of medium-dense soil gradually increases, and the inclination of loose soil gradually decreases. Finally, the failure angle of slip surface of medium-dense and loose soil both tends to be stable. Fig. 14 is a characteristic comparison diagram of the shear slip surface with different aspect ratios in the drum parabolic mode, in which Rankine's slip surface is added for comparison. The measured rupture angle of loose soil with limited width is greater than the ultimate rupture angle calculated by Rankine's method $\alpha = 45° + \varphi/2$. The measured rupture angle of medium-dense soil is smaller than Rankine's solution. The measured angle of loose soil with infinite width is close to or slightly smaller than Rankine's solution. In contrast, the measured angle of medium-dense soil with infinite width is close to or slightly greater than the angle calculated by Rankine's method.

For medium-dense soil, it is an infinite soil as B/H is 0.5, 0.6, and 0.7. When B/H is 0.5 and 0.6, there are two fracture surfaces. While B/H increases to 0.7, there is a slip surface and a more obvious soil arching effect [27, 28]. As shown in Fig. 13(c), the slip surface extends to the wall and soil surface junction with B/H=0.4, which can be regarded as a critical state. Therefore, 0.4 is the critical aspect ratio. The fracture surface of the broken line is more obvious with B/H=0.2,0.3.

For loose soil, it is an infinite soil as B/H is 0.5, 0.6, and 0.7. There are 2~3 rupture surfaces while the soil fails in its ultimate state. The slip surface extends to the junction of the wall and the filling surface with B/H=0.4. Thus, B/H=0.4 can be judged as the critical aspect ratio. When B/H is 0.2 and 0.3, there is a more apparent broken-line slip surface.

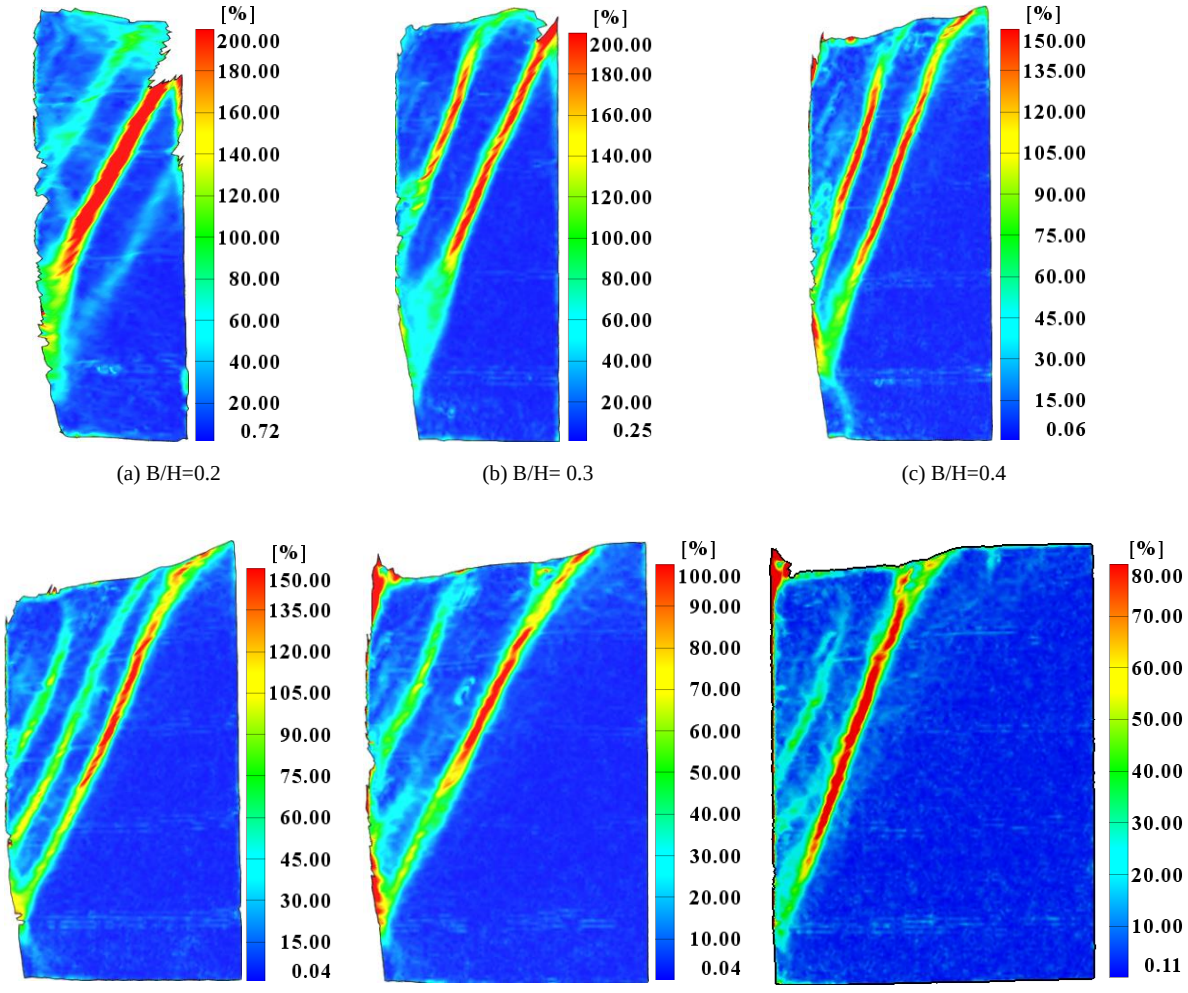

(a) B/H=0.2 (b) B/H= 0.3 (c) B/H=0.4

(d) B/H=0.5 (e) B/H=0.6 (f) B/H=0.7

Fig. 12. Loose soil shear strain cloud map under Drum-mode

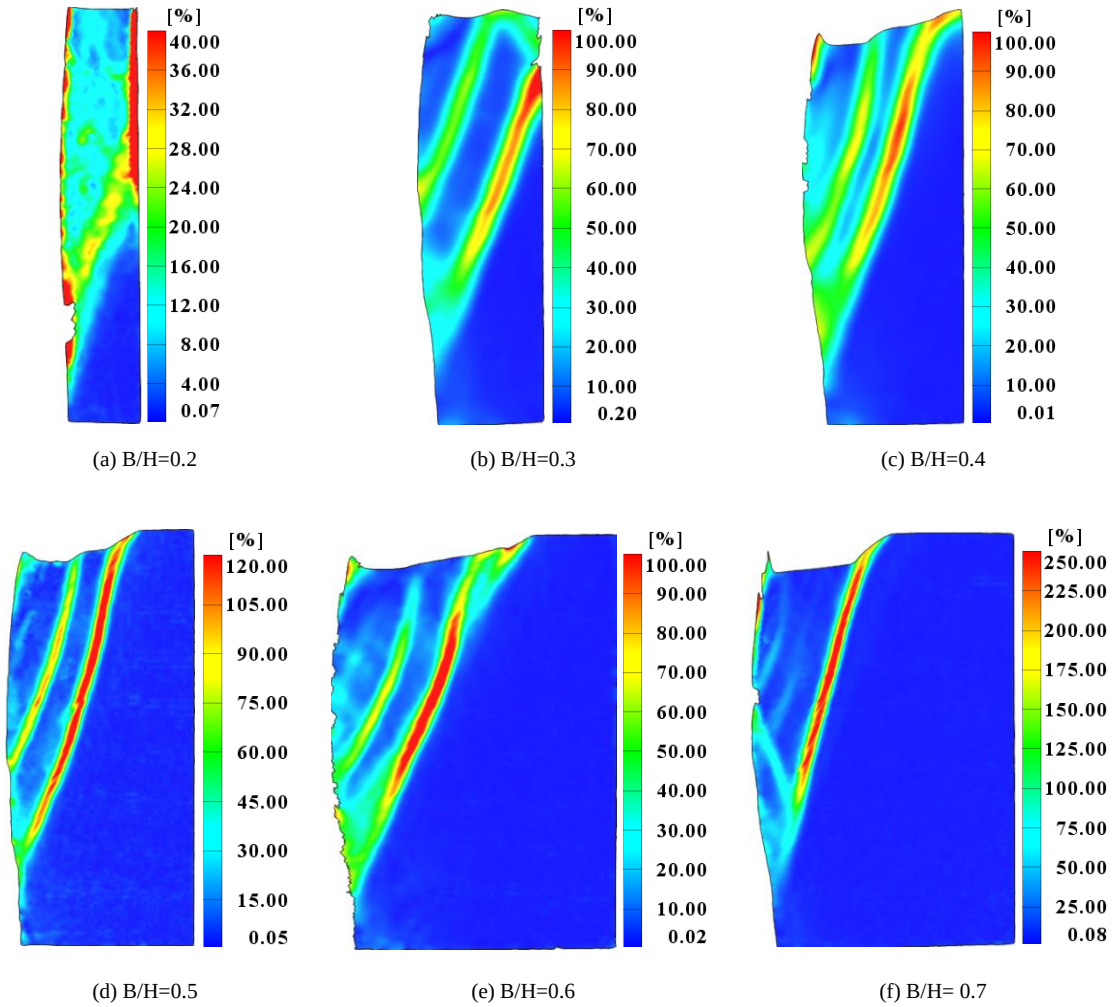

(a) B/H=0.2 (b) B/H=0.3 (c) B/H=0.4

(d) B/H=0.5 (e) B/H=0.6 (f) B/H= 0.7

Fig. 13. Medium dense soil shear strain cloud map under Drum-mode

(2) Soil Deformation

As shown in Fig. 15, for medium-dense soil with aspect ratios B/H=0.3, 0.4, 0.5, 0.6, and 0.7 (taking aspect ratio B/H=0.7 as an example), the maximal total displacement and the maximal displacement in the Y direction all appear near the top of the movable wall, the displacement magnitude gradually decreases downward. The total displacement nephogram has a good similarity with the vertical displacement nephogram. Maximal displacements in the X direction of medium-dense soils all occur at the central bulge. The settlement at the top of the soil is a groove settlement. The total displacement contours, vertical displacement contours, and horizontal displacement contours with B/H=0.3, 0.4, 0.5, 0.6, and 0.7 have good similarity. As shown in Fig. 16, the maximal total displacement and the maximal vertical displacement appear at the top of the soil layer while B/H is 0.2. The maximal displacement in the X direction still occurs in the middle of the wall. The total displacement map, X displacement, and Y displacement cloud map are not very similar.

As shown in Fig. 17, for loose soil, the aspect ratio B/H=0.6 is taken as an example. When the loose soil is deformed, the maximum horizontal displacement in the initial stage is raised in the middle of the wall. Then, the horizontal displacement of the top soil layer in the later stage increases rapidly. Finally, the maximum horizontal displacement of loose soil occurs near the top of a flexible retaining wall, and the horizontal displacement magnitude gradually decreases downward.

TABLE IV
FAILURE ANGLE OF SLIDING SURFACE (DRUM-MODE)

Failure angle(°)	B/H=0.2	0.3	0.4	0.5	0.6	0.7	45°+φ/2 (°)
Loose	66.0	65.2	66.6	64.4	60.4	61.5	61.95
Medium dense	60.3	63.4	65.3	66.7	67.3	68.9	65.95

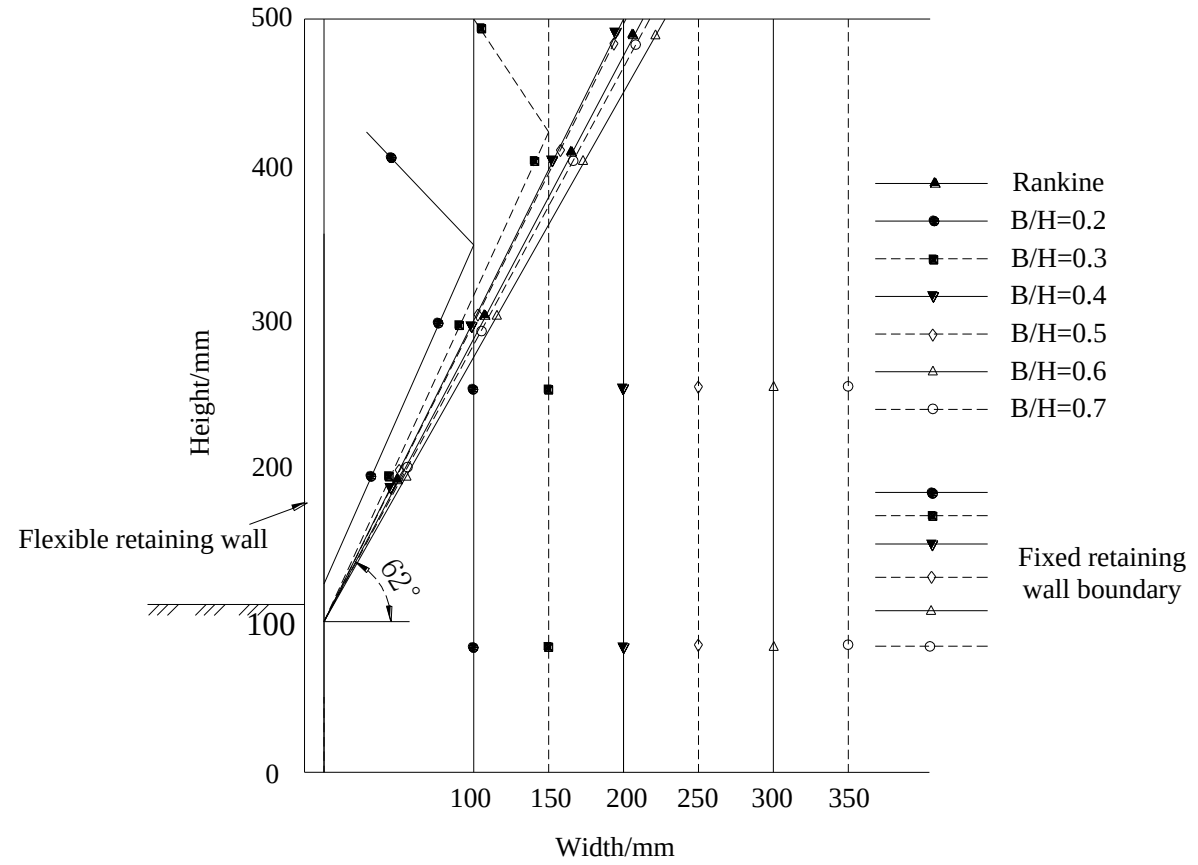

(a) Loose soil

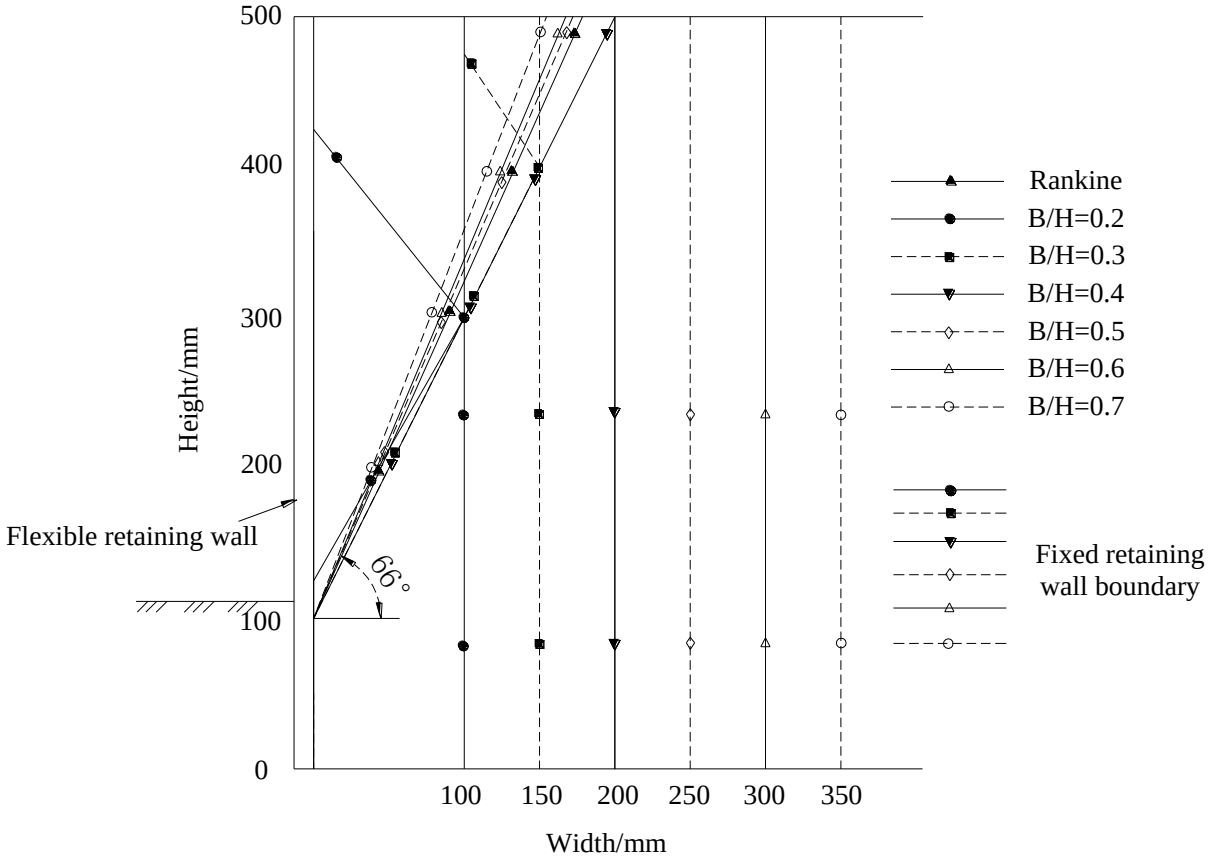

(b) Medium dense

Fig. 14. Characteristics of soil slip surface with different B/H under Drum-mode

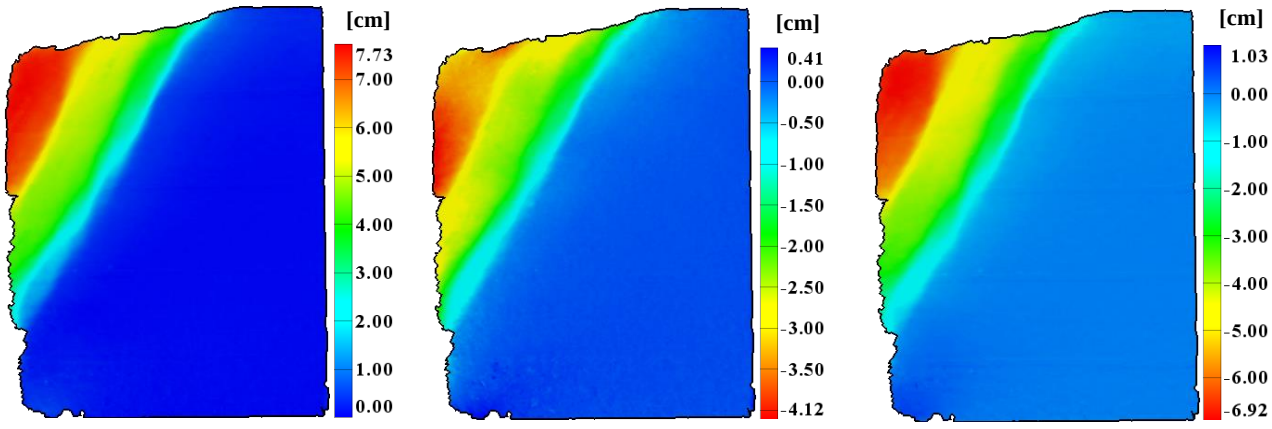

(a) Total displacement (loose) (b) X displacement (loose) (c) Y displacement (loose)

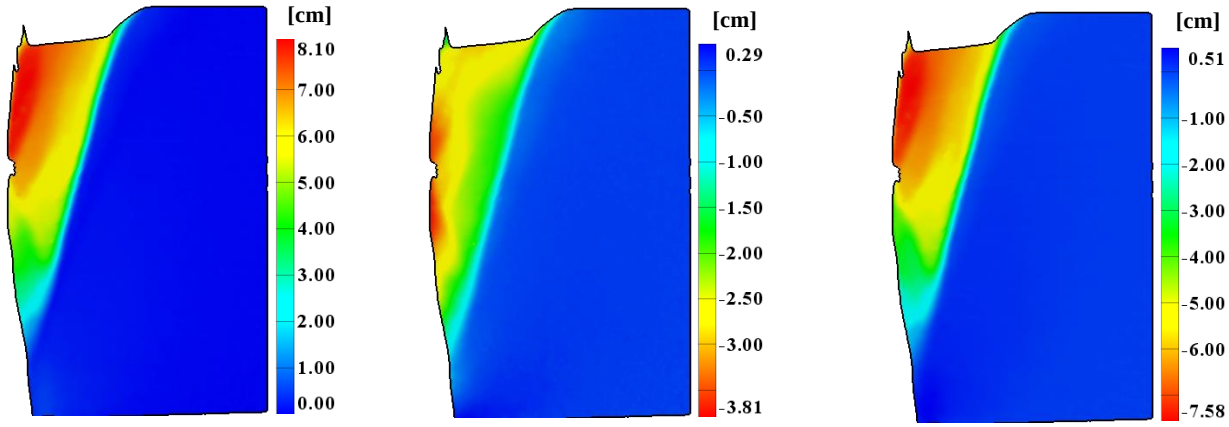

(d) Total displacement (Medium dense) (e) X displacement (Medium dense) (f) Y displacement (Medium dense)

Fig. 15. Soil deformation characteristics under Drum-mode (B/H=0.7)

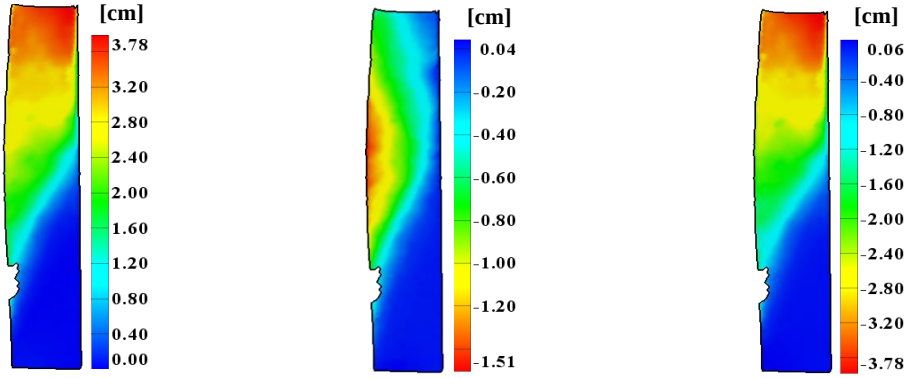

(a) Total displacement (b) X displacement (c) Y displacement

Fig. 16. Medium dense soil deformation characteristics under Drum-mode (B/H=0.2)

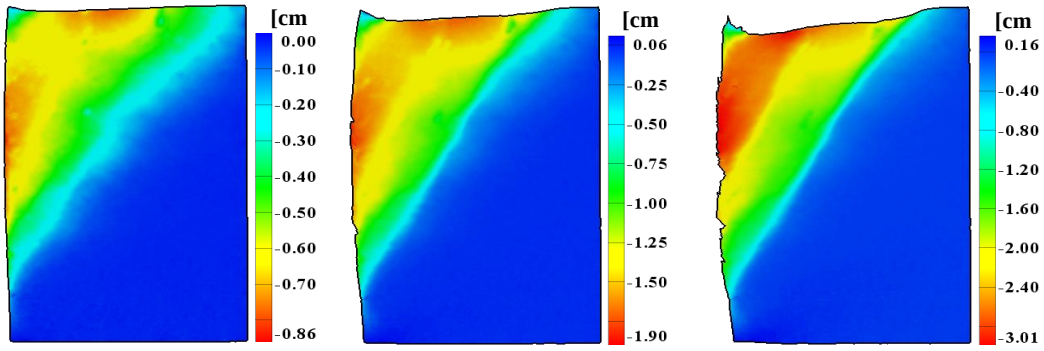

(a) Δx/x=20% (b) Δx/x=50% (c) Δx/x=100%

Fig. 17. Loose soil deformation characteristics under Drum-mode (B/H=0.6)

C. Test comparison and discussion

In RB mode of rigid retaining wall, the sliding area is not apparent, the rupture line is a right-sloping line, and the critical ratio is 0.6 [15,16]. In this paper, the sliding surface in the cantilever outward deflection mode is prominent and has a linear trend. The critical ratios in the cantilever outward deflection mode are 0.3 (medium-dense soil) and 0.4 (loose soil). Compared with RB mode of rigid retaining wall, the starting point of the sliding surface in cantilever outward deflection mode is higher, and there is a broken line sliding surface within limited width.

IV. Earth Pressure Distribution

The earth pressure distributions of medium-dense and loose soils with aspect ratios of 0.2, 0.3, 0.4, and 0.5 under cantilever outward deflection mode and drum parabolic mode were tested. The distribution law of earth pressure of medium-dense soil is described as follows.

A. Earth Pressure Distribution under Cantilever-Mode

As shown in Fig. 18, under the cantilever outward deflection mode, the earth pressure increases with the depth increase. As a result, the earth pressure on the upper soil layer is close to Rankine's solution. However, with the depth increase, the earth pressure on the lower soil layer exceeds Rankine's resolution. Because the lower part of the retaining wall is embedded and fixed, the deformation of the lower soil layer is small, and the earth pressure is larger.

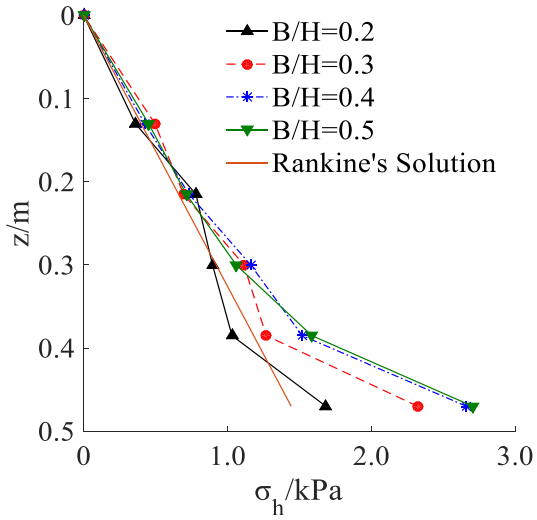

Fig. 18. Active pressure distribution along the height of retaining wall (Cantilever-mode)

Fig. 19 shows the variation of earth pressure along the retaining wall with the change of aspect ratio under the cantilever outward deflection mode. It can be seen that with the increase in aspect ratio, the earth pressure gradually increases. The growth is not evident after the critical aspect ratio is exceeded, which is basically stable.

B. Earth Pressure Distribution under Drum-Mode

As shown in Fig. 20, the earth pressure in the drum parabolic mode gradually increases with the depth. Because the support restrains the top of the retaining wall, the earth pressure in the upper part of the soil layer is greater than Rankine's solution. The deformation of the upper soil mass is small, resulting in a large earth pressure. The bulge in the middle of the soil layer has a large deformation, decreasing the earth pressure. Because the lower part of the retaining wall is embedded and fixed, the lower soil deformation is small. Therefore, the earth pressure at the lower part of the soil layer increases as the depth increases and gradually exceeds Rankine's solution.

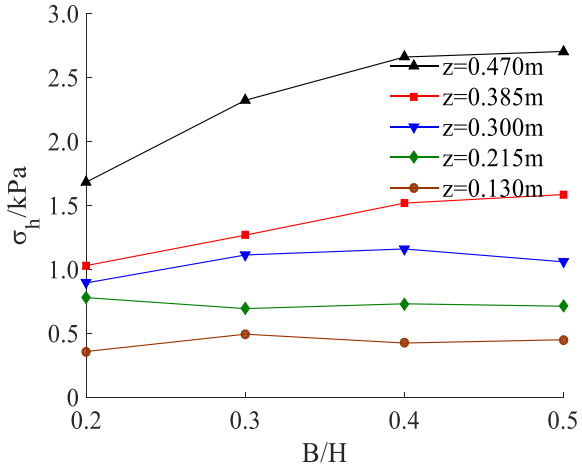

Fig. 19. Active pressure distribution with B/H (Cantilever-mode)

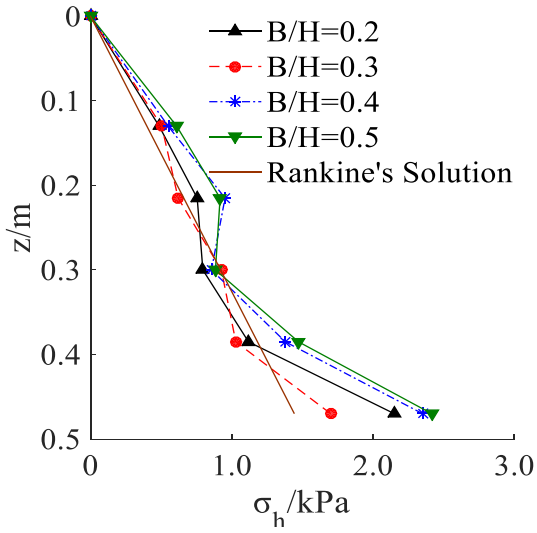

Fig. 20. Active pressure distribution along the height of retaining wall (Drum-mode)

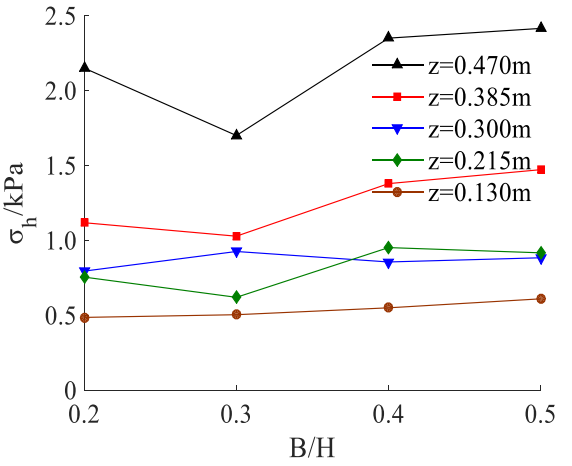

Fig. 21. Active pressure distribution with B/H (Drum-mode)

Fig. 21 shows the earth pressure along the retaining wall in the drum parabolic mode. It can be seen that with the increase of aspect ratio, on the whole, the earth pressure increases. But

after the critical aspect ratio is exceeded, the increase is not apparent, and the earth pressure values are relatively stable.

V. Conclusion

The self-made test equipment was used to simulate the cantilever outward deflection mode and the drum parabolic deformation mode of a flexible retaining wall. In addition, the model tests were conducted to explore the failure characteristics and the distribution law of active earth pressure of soil with limited width. As a result, the following conclusions are drawn.

(1) Under the Cantilever-mode of a flexible retaining wall, the sliding failure surface gradually forms a continuous straight line from top to bottom. The inclination of the rupture surface within limited width is larger than Rankine's solution. With the increase of B/H, the ultimate rupture angle gradually decreases and approaches Rankine's solution after reaching the infinite width. The critical aspect ratio is 0.4 for loose soil and 0.3 for medium-dense soil. When B/H is 0.2, the slip surfaces are broken-line slip surfaces.

(2) Under the Cantilever-mode of the flexible retaining wall, when the aspect ratio of loose and medium-dense soil is 0.3~0.7, the maximal total displacement, the maximal X-direction horizontal displacement, and the maximal Y-direction vertical displacement all appear near the top of the movable retaining wall; the cloud images in total displacement, horizontal displacement, and vertical displacement have a good similarity. However, when the aspect ratio is 0.2, the cloud images in total displacement, horizontal displacement, and vertical displacement are not similar.

(3) Under the Drum-mode of the flexible retaining wall, the slip surface develops from bottom to top and finally forms a continuously straight rupture surface. The rupture angle of loose soil with limited width is larger than Rankine's solution. In comparison, the rupture angle of medium dense soil is smaller than Rankine's solution. After entering the infinite width, the rupture angle is close to Rankine's solution. The critical aspect ratio is 0.4 for both loose and medium-dense soils. A relatively apparent broken line slip surface appears in the medium-dense soil with limited width.

(4) Under the drum-mode of a flexible retaining wall, when the aspect ratio is 0.3~0.7, the maximal total displacement and the maximal vertical displacement in the Y direction all appear near the top of the movable retaining wall, and the top settlement of soil mass is in the form of groove settlement. The maximal X-direction horizontal displacement of medium-dense soil occurs at the central bulge. In the first stage, the maximum horizontal displacement of loose soil bulges in the middle; then, the maximum horizontal displacement occurs near the top of the flexible retaining wall in the later stage.

(5) The earth pressure under the Cantilever-mode gradually increases with the depth. As a result, the earth pressure of the lower soil layer more significantly increases, exceeding Rankine's solution. Under the Drum-mode, the earth pressure along the retaining wall is distributed in an "R" shape. As a result, the earth pressures on the upper and lower soil layers exceed Rankine's solution, while the earth pressure on the middle soil layer is lower than Rankine's solution. In the Cantilever-mode and Drum-mode, with the increase of B/H, the earth pressure gradually increases and becomes a stable state after exceeding the critical aspect ratio.

Through the model test on failure characteristics and earth pressure distribution law in the Cantilever-mode and Drum-mode of flexible retaining walls, the study provides a valuable reference for the calculation of stability and the embedded depth of flexible retaining structures such as row pile, sheet pile, and diaphragm wall.

References

[1] M. X. Xie, J. J. Zheng, and R. J Zhang, "Active earth pressure on rigid retaining walls built near rock faces," International Journal of Geomechanics, vol.20, no.6, pp1-20, 2020.

[2] M. H. Yang, X. C. Tang, and Z. Y. Wu, "Slip surface and active earth pressure of cohesionless narrow backfill behind rigid retaining walls under translation movement mode, ". International Journal of Geomechanics, vol.20, no.8, pp1-9, 2020.

[3] C. C. Fan, and Y. S. Fang, "Numerical solution of active earth pressures on rigid retaining walls built near rock faces," Computers and Geotechnics, vol.37, pp1023-1029, 2010.

[4] V. Greco, "Active thrust on retaining walls of narrow backfill width," Computers and Geotechnics, vol.50, pp66-78, 2013.

[5] X. Y. Liu, Y. Zhang, and K. J. Zhang, "Optimization Control of Energy Consumption in Tunneling System of Earth Pressure Balance Shield Tunneling Machine," Engineering Letters, vol. 28, no.2, pp551-558, 2020

[6] X. Y. Liu, C. Y. Zhou, Y. D. Wang, and Q. M. Cong, "Data-driven Optimal Control of Earth Pressure Balance for Shield Tunneling Machine," Engineering Letters, vol. 29, no.4, pp1436-1444, 2021

[7] K. H. Yang, K. T. Kniss , and S. G. Wright, "Finite Element Analyses for Centrifuge Modelling of Narrow MSE Walls," The First Pan American Geosynthetics Conference&Exihibition, Cancun. Mexico: pp1623-1630, 2008.

[8] S. Frydman, and I. Keissar, "Earth pressures on retaining walls near rock faces. Journal of Geotechnical Engineering," ASCE, vol. 113, no.6, pp586-599, 1987.

[9] W. A. Take, and A. J. Valsangkar, "Earth pressures on unyielding etaining walls of narrow backfill width," Journal of Canadian Geotechnical, vol.38, pp. 1220-1230, 2001.

[10] M. H. Khosravi, T. Pipatpomgsa, and J. Takemura, "Experimental analysis of earth pressure against rigid retaining walls under translation mode," Géotechnique, vol.63, no.12, pp1020-1028, 2013.

[11] M. H. Yang, X. B. Dai, and M. H. Zhao, "Experimental study on active earth pressure of cohesionless soil with limited width behind retaining wall," Chinese Journal of Geotechnical Engineering, vol.38, no.1, pp131-137, 2016.

[12] W. Zhu, "Experimental and theoretical study on earth pressures considering limited soils and retaining wall deformation," [D]. Hangzhou: Zhejiang University, 2014.

[13] W. D. Hu, L. X. Zeng, and X. H. Liu, "Active earth pressures against rigid retaining walls for finite soil in grading condition," Hydrogeology & Engineering Geology, vol.45, no.6, pp63-70, 2018.

[14] T. Fang, S. H. Sun, and C. J. Xu, "Earth pressure experimental study of limited soil considering the mode of displacement of retaining wall," Journal of Railway Science and Engineering, vol.16, no.5, pp1178-1185, 2019.

[15] C. Y. Wang, X. P. Liu, Z. H. Cao, X. Jiang, and J. Q. Zhang, "Experimental study on active slip surface of limited width soil behind rigid wall, " Rock and Soil Mechanics.vol.42, no.11, pp 2943-2952, 2021.

[16] C. Y. Wang, X. P. Liu, J. Q. Zang, and Z. H. Cao, "Experimental study on passive slip surface of limited width soil behind rigid wall," Rock and Soil Mechanics, vol.42, no.7, pp1839-1849, 2021.

[17] H. W. Ying, J. H. Zhang, and X. G. Wang, "Experimental analysis of passive earth pressure against rigid retaining wall under translation mode for finite soils," Chinese Journal of Geotechnical Engineering, vol.38, no.6, pp978-986, 2016.

[18] W. D. Hu, X. N. Zhu, X. H. Liu, Y. Q. Zeng, and X. Y. Zhou, "Active Earth Pressure against Cantilever Retaining Wall adjacent to Existing Basement exterior Wall," International Journal of Geomechanics.vol.20, no.11, pp1532-3641, 2020.

[19] X. S. Cheng, G. Zheng, and T. M. Huang, "Experimental study on mechanism of progressive collapse along length of excavation retained by cantilever contiguous piles," Chinese Journal of Geotechnical Engineering, vol.38, no.9, pp1640-1649, 2016.
[20] H. W. Ying, B. B. Zheng, and X. Y. Xie, "Study of passive earth pressures against translating rigid retaining walls in narrow excavations," Rock and Soil Mechanics, vol. 32, no.12, pp3755-3762, 2011.
[21] P. Y. Lu, C. Yan, and X. L. Gu, "Sand model test on the distribution of earth pressure," China Civil Engineering Journal, vol.36, no.10, pp84-88, 2003.
[22] W. D. Hu, X. N. Zhu, and X. Y. Zhou, "Experimental study on passive earth pressures of cohesionless soils with limited width against cantilever piles flexible retaining walls, " Chinese Journal of Rock Mechanics and Engineering, vol.38, no.Suppl.2, pp3748-3757, 2019.
[23] X. N. Zhu, Y. Q. Zeng, W. D. Hu, X. H. Liu, and X. Y. Zhou, "Experimental Study on Passive Earth Pressure against Flexible Retaining Wall with Drum Deformation," Engineering Letters, vol. 29, no.2, pp339-350, 2021.
[24] T. Daiki, L.Nicolas, and O. Jun, "Localised deformation in a wide-grained sand under triaxial compression revealed by X-ray tomography and digital image correlation," Soils and Foundations, vol.55, no.4, pp906-915, 2015.
[25] L. Lin, C. S. Tang, and Q. Cheng, "Desiccation cracking behavior of soils based on digital image correlation technique," Chinese Journal of Geotechnical Engineering, vol.41, no.7, pp1311-1318, 2019.
[26] D. J. White, W. A. Take, and M. D. Bolton, "Soil deformation measurements using particle image velocimetry (PIV) and photogrammetry," Géotechnique, vol.53, no.7, pp619-631, 2003.
[27] Z. Y. Huang, Y. X. Zhang, and J. Dong, "Experimental study of soil arching and transfer behavior of earth pressure about sheet-pile walls," Rock and Soil Mechanics, vol.34, no.7, pp1887-1892, 2013.
[28] M. H. Yang, Z. Y. Wu, and M. H. Zhao, "Soil arch effect analysis and earth pressure calculating method for finite width soil behind retaining wall," Journal of Hunan University (Natural Sciences), vol. 47, no.3, pp19-27, 2020.

Mr. Xinnian Zhu was born in November 1975 and received his B.E. degree and M.S. Degree from Hunan University, Changsha, China, in 1999 and 2010, respectively. His research interests are mainly on slope support and earth pressure test for foundation pit engineering. Xinnian Zhu has worked as a lecturer in Hunan Institute of Science and Technology. He has authored or co-authored 5 journal papers and 3 international conference papers to date.

Dr. Weidong Hu received the Ph.D. degree from Hunan Univesrtiy, Changsha, China, in 2016. Hu is the professor of College of Civil Engineering and Architecture, Hunan Institute of Science and Technology, Yueyang, China. His research interests cover excavation engineering and earth pressure. He has published more than 40 technical papers.

Dr. Yongqing Zeng was born in February 1991 and received his M.S. Degree from Anhui University of Science and Technology, Huainan, China, in 2016, and received the Ph.D. degree from Institute of Rock and Soil Mechanics, Chinese Academy of Sciences, Wuhan, China, in 2019. Yongqing Zeng has worked as a lecturer in Hunan Institute of Science and Technology. He authored or co-authored 15 journal papers and 4 international conference papers to date.

Tao Hu was born in November 1999 and received his B.E. degree from Hunan City University, Yiyang, China, in 2021. He is studying for a master's degree in College of Civil Engineering and Architecture, Hunan Institute of Science and Technology, Yueyang, China. His research interests are mainly on slope support and earth pressure test for foundation pit engineering. He has authored or co-authored 1 journal papers.

Siqing Jiang was born in January 2000 and received his B.E. degree from Nanhu College, Hunan Institute of Science and Technology, Yueyang, China, in 2021. In the same year, he entered College of Civil Engineering and Architecture, Hunan Institute of Science and Technology for a master's degree. His research interests are mainly on slope support and earth pressure test for foundation pit engineering.

Mr. Weiwei Wang was born in April 1986 and received the M.S. Degree from Changsha University of Science and Technology, Changsha, China, in 2013. His research interests are mainly on calculation of earth pressure on the retaining wall. He has authored or co-authored 6 journal papers to date.